Stoch Environ Res Risk Assess (2014) 28:2161–2173
DOI 10.1007/s00477-014-0872-9

ORIGINAL PAPER

Climate extremes in South Western Siberia: past and future

Degefie T. Degefie · Elisa Fleischer · Otto Klemm · Andrey V. Soromotin · Olga V. Soromotina · Andrey V. Tolstikov · Nikolay V. Abramov

Published online: 16 April 2014

Abstract In this study, the temporal and spatial trends of ten climate extreme indices were computed based on observed daily precipitation and on daily maximum and minimum temperatures at 26 weather stations in South Western Siberia during the period 1969–2011 and, based on projected daily maximum and minimum temperatures, during 2021–2050. The Mann–Kendall test was employed to analyze the temporal trend and a combination of multiple linear regressions and semivariogram functions were used to evaluate the regional spatial trends and the local spatial variability of climate extremes, respectively. The results show that the temperature-based climate extremes increase at a 0.05 significance level while none of the precipitation-based climate extremes did. Spatially, dominant gradients are observed along latitude: The northern taiga vegetation zone experiences a colder and wetter climate while the southern forest steppe zone is drier and hotter. Over time, a tendency towards homogenization of the regional climate is observed through a decrease of the spatial variability for most climate extreme indices. In the future, the most intense changes are anticipated for the bioclimate indicators "growing season length" and "growing degree days" in the north, while the warming indicators, "warm day" and "warm night" are expected to be high to the south.

Keywords Climate extremes · Global warming · Climate change · South Western Siberia

D. T. Degefie (✉) · E. Fleischer · O. Klemm
Climatology Working Group, Institute of Landscape Ecology, University of Münster, 48149 Münster, Germany
e-mail: degefie.tibebe@uni-muenster.de

A. V. Soromotin · O. V. Soromotina
Research Institute of Ecology and Natural Resources Management, Tyumen State University, Przhevalski Str. 37a, Tyumen 625003, Russia

A. V. Tolstikov
Tyumen State University, Semakova Str. 10, Tyumen 625023, Russia

N. V. Abramov
State Agrarian University of the Northern Trans-Urals, Respublika Str. 7, Tyumen 625003, Russia

1 Introduction

Global warming is a major phenomenon since the beginning of the industrial era. The observed increase of anthropogenic greenhouse gas emissions into the atmosphere is considered to be the main cause for the increase of the global average temperature from the mid-twentieth century on Intergovernmental Panel on Climate Change, IPCC (2007a). According to the 2007 report of the IPCC (2007b), ocean warming, continental average temperature increase, temperature extremes, and wind patterns are other aspects of climate which are influenced by human activity. These changes in climate, which are often characterized through shifts of the respective mean states (for example, an increase of the mean temperature), are closely related to changes in the frequency, intensity, spatial extent, duration, and timing of weather and climate extremes. This may result in unprecedented extremes (IPCC 2012).

Numerous studies on climate extremes in various parts of the world show that extreme weather events have been becoming more frequent and more intense, and are likely to become even more frequent, more widespread, and/or more intense during the twenty first century (IPCC 2007b). Studies in Western Siberia about climate change indicate an increase of the average

temperature of the vegetation period by more than 1 °C over the last 15 years, coupled with a prolonged growing season (Frey and Smith 2003). An increase in winter precipitation was also observed along with strong and prevalent springtime warming. Another study by Shulgina et al. (2011) revealed a decrease of the duration of the cold season over most of the Western Siberia territories by 1–3 days per decade. A corresponding increase of the growing season length (GSL) by 2–4 days per decade was reported in the same study.

The impact of climate extremes is largely manifested by disasters such as floods, drought, heat waves, or fire. This happens when the frequency or the intensity (or both) of climate extremes cross critical thresholds in a physical, ecological, or social system. For instance, heat waves may control biogeochemical processes such as carbon and nitrogen cycling and eventually modify the function and service of an ecosystem. A study by Arnone et al. (2008) observed a decrease of the CO_2 uptake of a terrestrial ecosystem due to more frequent warm years.

Western Siberia is a region of global importance due to the massive amounts of carbon stored in the soil system and due to its large biodiversity. The recent increase of global warming could potentially alter the climate of the region and consequently affect its ecosystem services and natural resources. A study in neighboring northern Kazakhstan indicates an increase of drought risk, which is anticipated to spread towards to South-Western (SW) Siberia (Pilifosova et al. 1997). This tendency could trigger a northward shift of the Western Siberian grain-belt into the forest steppe and pre-Taiga zone. A potential risk associated with the climate change in the region lies in the increase of the risk of forest fires and burning of peatland during dry periods in the south. Forest and peatland fires lead to a release of carbon from the trees and soil into the atmosphere. This alters the radiative balance and contributes to further global warming.

This study attempts to analyze the temporal and spatial trends of climate extremes in a much more detailed analysis than was performed before. Particular focus lies on the analysis of local scale spatial variability of climate extremes. Do spatial gradients within the region intensify over time? How closely are regional climate extreme trends connected to large scale atmospheric pattern? Segregation of large scale from regional phenomena will help to understand and to evaluate regional climate dynamics and to develop adaptation strategies.

2 Data and methods

2.1 Data

Observed and projected meteorological data of 26 weather stations in the region were used for the study (Fig. 1). Lengths of the measurement period, the completeness of recorded data, and the evenness of the spatial distribution in the region were the main criteria for selecting the stations. Complete coverage of the ecological zones in the area (Table 1) was another criterion. The recording periods vary from station to station. For this analysis, we considered years which are common across all stations. Therefore, historical weather data between 1969 and 2011 were fully considered for computing climate extremes and further analysis.

The National Climate Data Center archive (ftp://ncdc.noaa.gov/pub/data/ghcn/daily/) was the main source for historical weather data. Moreover, climate data from Tu Tiempo[1] were used to supplement the dataset. The daily precipitation amount and the daily maximum and minimum temperatures were used.

Various quality control steps were applied to identify erroneous data and outliers and to code missing values. Moreover, homogeneity tests and adjustments as recommended by the Expert Team on Climate Change Detection and Indices (ETCCDI) were applied using the RHTest program, which is developed within the R Package (http://etccdi.pacificclimate.org/software.shtmll) specifically for time series quality assurance purposes.

A statistical downscaling method (SDSM 4.2) was used to downscale and project point based daily data (minimum and maximum temperatures) until the year 2100. The SDSM was employed in this study to establish statistical relationship between general circulation model (GCM) predictors and local climate variables. The statistical relationship can be written as:

$$P = f(G),$$

in which P is the predict and (a local climate variable, e.g., minimum and maximum temperature), G is the predictor (a set of large-scale climate variables, e.g., 500/850-hPa geopotential height or mean sea level pressure), and f is a deterministic or stochastic function that has to be estimated from historical observations. Accordingly, multiple regressions were developed based on the daily GCM predictors (1961–2000) as derived from the CGCM3.1 A2 (www.cccma.ec.gc.ca/data/cgcm3_t63_sresa) and from historical data of the weather stations that were located in the same spatial domain as the respective grid boxes of large scale GCM predictors. Historical weather stations data from 1961 to 1990 and from 1991 to 2000 were used during calibration and validation of the regression equations, respectively. After calibration and validation, the regression equations were used to project the future climate variables based on the daily GCM predictor data, derived

[1] Tu Tiempo is a private company organizing and storing global historical weather data (www.tutiempo.net).

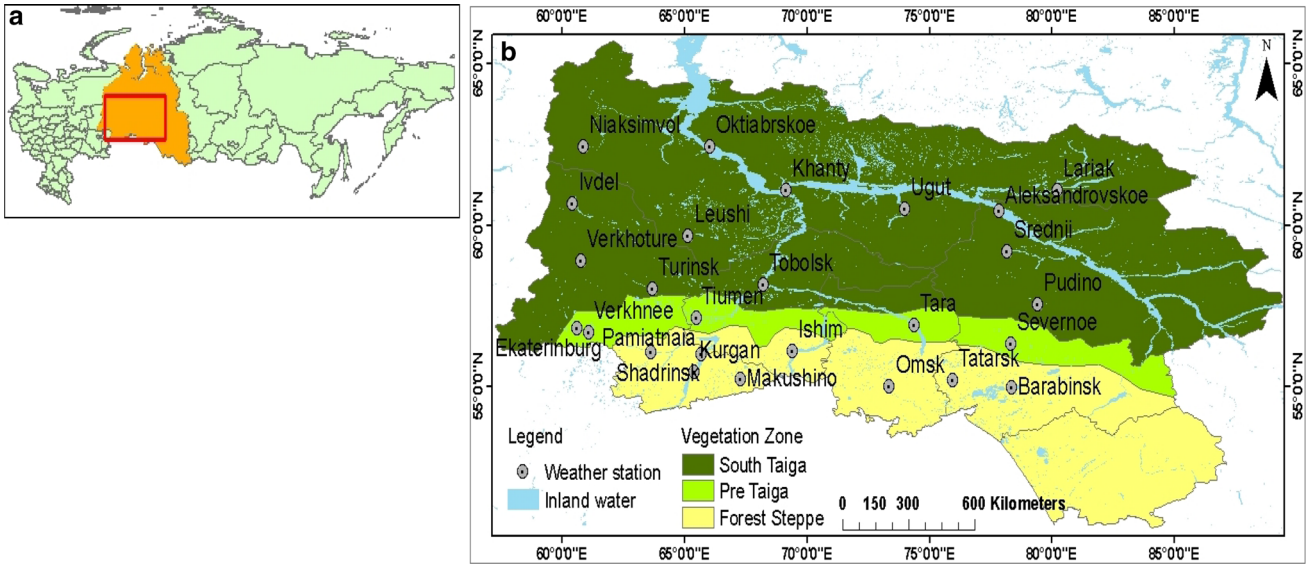

Fig. 1 Map of (**a**) Russian Federation as a reference to the study area, and (**b**) weather station distribution in South Western Siberia

from the CGCM3.1 A2 SRES scenario (www.cccma.ec.gc.ca/data/cgcm3_t63_sresa).

The A2 SRES emission scenario assumes that regional heterogeneity, self-reliance of various regions and local identities are emphasized over the next 100 years and that economic development is regionally oriented. It is realistic to consider this emission scenario for a study such as this present one, focusing on regional and local levels.

2.2 Methods

2.2.1 Climate extreme indices

There are numerous methods and indicators to assess climate extremes in a changing climate. We refer to the tool developed by the ETCCDI, which is a joint expert team from CCl[2]/CLIVAR[3]/JCOMM[4] (WMO 2009). The tool uses sixteen temperature-related indices and eleven precipitation-related indices to extract the occurrence of extreme events in a meteorological time series. These 27 indices can be calculated by the RClimDex program, which is developed specifically for this purpose within the R Package (http://etccdi.pacificclimate.org/list_27_indices.shtml). Ten indices were selected for this study, taking into account their robustness, their little correlation with each other, and their potential to exert impact on ecosystems and human society (Table 2). In addition, the number of growing degree days (GDDs), which is not included in the standard definitions of indices, was used.

[2] CCL stands for WMO's commission for Climatology.

[3] CLIVAR stands for Climate Variability and Predicibility.

[4] JCOMM stands for for WMO-IOC Technical Commission for Oceanography and Marine Meteorology.

The temperature-based indices are grouped into extreme value indices, relative indices, and absolute indices (Table 2). Extreme value indices are indices that utilize extreme values of the daily maximum and minimum temperatures. Relative indices are computed based on relative or floating thresholds. In the calculation of these indices, the 90th (10th) percentile of the daily maximum (minimum) temperature data of the reference period are taken as the upper (lower) threshold. Absolute indices are computed based on original observational data and fixed thresholds. In the same fashion, the precipitation-based indices are grouped into relative and absolute indices (Table 2).

All the above 10 indices were computed using observed and projected climate data of the 26 stations.

2.2.2 Temporal trend

2.2.2.1 Mann–Kendall A non-parametric rank-based Mann–Kendall (MK) trend test (Mann 1945; Kendall 1975) was applied to climate extreme indices. It was applied for each station as well as for the region as a whole after averaging indices of all stations. The MK test is commonly used for detecting monotonic increases and decreases in meteorological time series (Gemmer et al. 2011; Vincent et al. 2011; Wang et al. 2012; Yang et al. 2011). In a trend test, the null hypothesis H0 is that there is no trend in the analyzed time-series, and hypothesis H1 is that there is a trend in the analyzed data. The MK test is applied by considering the statistic S as:

$$S = \sum_{n=1}^{n-1} \sum_{j=k+1}^{n} \operatorname{sgn}(X_j - X_k),$$

where X_j and X_k are the annual values in years j and k, $j > k$, respectively, and

Table 1 Climate characteristics of the weather stations and ecological zones

Numbers	Station name	Latitude (°)	Longitude (°)	Altitude (m)	Mean annual precipitation (mm)	Mean temperature (°C)		Vegetation zones
						T_{max}	T_{min}	
1	Shadrinsk	56.08	63.63	88	455.5	7.8	−1.8	Forest steppe
2	Pamiatnaia	56.02	65.70	66	388.0	7.1	−3.4	
3	Ishim	56.10	69.43	81	401.3	6.6	−3.7	
4	Kurgan	55.47	65.40	73	385.6	7.7	−2.4	
5	Makushino	55.25	67.30	140	362.2	7.1	−2.5	
6	Omsk	55.02	73.38	121	411.6	6.9	−2.9	
7	Tatarsk	55.20	75.97	110	378.7	7.2	−3.3	
8	Barabinsk	55.00	78.37	119	387.7	6.4	−3.7	
9	Tiumen	57.15	65.50	79	476.2	7.0	−2.8	Pre-Taiga
10	Ekaterinburg	56.83	60.63	281	517.9	7.4	−1.0	
11	Verkhnee	56.70	61.10	286	546.0	6.9	−2.1	
12	Tara	56.90	74.39	73	446.3	5.8	−4.4	
13	Severnoe	56.35	78.35	124	465.8	5.8	−4.6	
14	Niaksimvol	62.43	60.87	51	525.6	3.7	−6.6	South Taiga
15	Oktiabrskoe	62.45	66.05	70	614.1	2.5	−6.0	
16	Lariak	61.10	80.25	55	544.8	2.1	−7.1	
17	Ivdel	60.68	60.45	93	529.5	5.2	−5.6	
18	Khanty	61.07	69.17	46	544.0	3.3	−5.0	
19	Ugut	60.50	74.02	47	584.3	2.8	−6.5	
20	Aleksandrovskoe	60.43	77.87	47	511.6	3.4	−6.2	
21	Leushi	59.67	65.17	70	495.2	5.1	−3.6	
22	Verkhoture	58.90	60.79	125	558.6	6.6	−3.7	
23	Turinsk	58.04	63.70	103	520.3	6.7	−3.1	
24	Tobolsk	58.15	68.25	49	479.3	5.6	−4.0	
25	Srednii	59.20	78.20	68	547.7	4.8	−5.1	
26	Pudino	57.57	79.43	96	503.1	5.8	−5.6	

The station name transliterated after ICAO, passport 2013

$$\operatorname{sgn}(X_j - X_k) = \begin{vmatrix} +1 (X_j - X_k) > 0 \\ 0 (X_j - X_k) = 0 \\ -1 (X_j - X_k) < 1 \end{vmatrix}.$$

The MK test has two parameters. One is the significance level that indicates the test strength and the other one is the slope magnitude estimate that indicates the direction of the trend. Under the null hypothesis, x_i are independent and randomly ordered, the statistic S is approximately normally distributed when $n \geq 8$ with zero mean and variance as $Var(S) = n(n-1)(2n+5)/18$. The standardized statistical test (Z) was computed by:

$$Z = \begin{vmatrix} \frac{S-1}{\sqrt{Var(S)}} & S > 0 \\ 0 & S = 0 \\ \frac{S+1}{\sqrt{Var(S)}} & S < 0 \end{vmatrix}.$$

At the given significance level α, if $|Z| \geq Z_{1-\alpha/2}$, the H0 is rejected, that means the time-series has a trend in the MK test at significance level α. Furthermore, if $Z > 0$, the time-series has an upward trend, and if $Z < 0$, it has a downward trend.

2.2.3 Spatial gradient

The regional and local spatial gradient of the climate extreme indices were examined on decadal bases using multiple linear regressions and a geostatistical function called semivariogram, respectively. The decades are, 1971–1980, 1981–1990, 1991–2000, 2001–2010, 2011–2020, 2021–2030, 2031–2040, and 2041–2050.

The multiple linear regressions were used to identify the significant regional spatial gradient of the decadal climate extreme indices along latitude and longitude. Furthermore,

Table 2 Climate Extreme Indices used in this study

Elements	Index	Indicators	Definitions	Units
Temperature				
Extreme value indices				
	TXx	Maximum value of maximum temperature	Maximum value (x) of the daily maximum temperature (TX) in each year	°C
	TNn	Minimum value of minimum temperature	Minimum value (n) of the daily minimum temperature (TN) in each year	°C
Relative indices				
	TN90p	Warm nights	Percentage of days when TN >90th %, percentage of time in base period (1969–2011)	% Days
	TX90p	Warm days	Percentage of days when TX >90th %, percentage of time in base period (1969–2011)	% Days
Absolute indices				
	GSL	Growing season length	Annual (1 Jan–31 Dec) count of days between first and last periods, during which six consecutive days occurred with daily mean temperature TG >5 °C	Days
	GDD	Growing degree days	Sum of temperature $\left(\frac{TX+TN}{2}\right) - T_{base}$ within the growing season (T_{base} = 5 °C, the lowest temperature where metabolic processes result in a net substance gain in above ground biomass)	Degree-days
Precipitation				
Relative indices				
	R95p	Very wet days	Annual total precipitation when daily precipitation amount (RR) >95 % percentage of time in base period (1969–2011)	mm
Absolute indices				
	Rx5day	Max 5-day precipitation amount	Monthly maximum consecutive 5-day precipitation	mm
	CDD	Consecutive dry days	Maximum number of consecutive days with daily precipitation amount (RR) <1 mm	Days
	R10	Number of heavy precipitation days	Annual count of days when $PRCP$ >10 mm	Days

the residuals of the fitted regression model were used to evaluate the local spatial variability by applying a semivariogram function. Maps were prepared by interpolating the multiple linear regression models and kriging of the residuals through geo-statistical functions. Final maps were produced by summing the maps that are made from the two functions.

2.2.3.1 Multiple linear regressions The regional spatial gradient analysis includes fitting a two-dimensional least square surface along latitude and longitude as:

$$Y = b + a_1x_1 + a_2x_2,$$

where Y represents the least square value of the particular climate extreme index and x_1 and x_2 represent the longitude and latitude dimensions along which the least square trend surface is computed. The slopes a_1 and a_2 indicates the spatial gradient of the climate indices along longitude and latitude which are computed in decadal basis. Spatial gradient are obtained for each extreme index on decadal basis and the statistical significance P of the trends was assessed by applying the t-statistics in both dimension.

2.2.3.2 Semivariogram The semivariogram is the geostatistical key function that is used to characterize the local spatial variability of climate extremes as based on the residuals obtained from the multiple linear regression function. The experimental semivariogram $\gamma(h)$ of the residue were computed as half the average squared difference between data pairs belonging to a certain distance class:

$$\gamma(h) = \frac{1}{2N(h)}\sum_{\alpha=0}^{N(h)}[Z(u_\alpha) - Z(u_\alpha + h)]^2,$$

where $N(h)$ is the number of the data pairs, $Z(u_\alpha)$ and $Z(u_\alpha + h)$, available from the n measurements, given n measurements $[Z(u_\alpha),\ \alpha = 1,\ \ldots,\ n]$ from a single realization.

Sill, partial sill, nugget and range are the semivariogram parameters, as Fig. 2 presents, that determine the spatial pattern of the climate extreme index in a given period.

In this study, rang values, which were computed on decadal basis, were taken as an indicator for the temporal

Table 3 Linear trend of the six temperature-based and four precipitation-based climate extremes for individual stations on observed data (1969–2011)

Numbers	Station names	Linear trends									
		TNn	*TXx*	*TN90p*	*TX90p*	GSL	GDD	*R10*	CDD	*R×5day*	*R95p*
1	Shadrinsk	**0.16**	0.01	***0.73***	***0.64***	0.27	***7.75***	**0.09**	−0.22	**0.39**	0.1
2	Pamiatnaia	**0.12**	0.01	***0.6***	***0.78***	**0.46**	***5.67***	−0.02	−0.09	−0.02	−0.02
3	Ishim	***0.15***	0.01	***0.86***	***0.8***	**0.43**	***8.14***	0.01	−0.26	−0.44	−0.01
4	Kurgan	**0.13**	0.03	***0.65***	***0.75***	**0.37**	***6.82***	−0.01	−0.21	−0.19	−0.04
5	Makushino	0.09	0.04	***0.85***	***0.93***	0.26	–	0.01	0.23	0.18	0.01
6	Omsk	**0.1**	−0.02	***0.76***	***0.64***	**0.41**	***5.52***	−0.01	0.21	0.1	0.08
7	Tatarsk	**0.13**	−0.03	***0.68***	***0.78***	**0.45**	***5.82***	0.01	0.2	0.27	0.08
8	Barabinsk	0.08	−0.02	***0.93***	***0.65***	**0.62**	***4.93***	−0.02	0.08	0.03	−0.01
9	Tiumen	***0.18***	0.02	***0.76***	***0.74***	**0.46**	***7.89***	0.05	0.22	−0.32	0.03
10	Ekaterinburg	***0.2***	**0.05**	***0.84***	***0.53***	0.4	***7.23***	0.05	−0.28	0.19	0.06
11	Verkhnee	**0.17**	0.03	***0.88***	***0.49***	−0.1	***6.11***	0.07	−0.12	−0.3	0.11
12	Tara	**0.1**	0.02	***0.64***	***0.69***	0.38	***4.62***	***−0.16***	−0.2	**−0.37**	−0.03
13	Severnoe	0.09	0	***0.86***	***0.84***	**0.86**	***7.23***	0.03	0.29	0.15	−0.02
14	Niaksimvol	***0.18***	0.04	***0.6***	0.35	**0.44**	**3.73**	0.02	−0.14	−0.18	−0.04
15	Oktiabrskoe	***0.16***	**0.05**	***0.78***	***0.69***	**0.75**	***5.72***	−0.04	0.05	−0.04	−0.03
16	Lariak	**0.12**	0.02	***0.83***	***0.92***	**0.75**	***5.3***	0.04	0.08	−0.03	0.04
17	Ivdel	***0.15***	**0.05**	***0.68***	**0.47**	**0.44**	***5.79***	0.03	−0.27	−0.02	0.01
18	Khanty	***0.15***	**0.05**	***0.76***	***0.61***	**0.88**	***5.76***	−0.05	−0.05	−0.58	−0.07
19	Ugut	***0.15***	−0.05	***0.84***	***0.67***	**1.15**	***6.05***	−0.05	−0.09	0.11	−0.08
20	Aleksandrovskoe	**0.11**	0	***0.62***	***0.69***	**0.89**	***5.36***	0.03	−0.02	−0.26	0.00
21	Leushi	***0.14***	**0.06**	***0.7***	***0.58***	0.45	***5.98***	0.00	−0.03	−0.41	0.08
22	Verkhoture	***0.17***	**0.04**	***0.65***	***0.57***	**0.4**	***6.31***	0.02	−0.35	−0.05	−0.03
23	Turinsk	***0.19***	**0.04**	***0.82***	***0.66***	**0.54**	***7.94***	0.01	−0.15	0.37	0.05
24	Tobolsk	**0.11**	0.02	***0.69***	***0.8***	**0.49**	***5.29***	0.04	0.01	−0.13	0.01
25	Srednii	0.1	0	***0.65***	***0.56***	**0.85**	***5.22***	−0.02	−0.3	−0.18	−0.01
26	Pudino	0.07	−0.04	***0.64***	***0.56***	**0.76**	***4.52***	0.00	−0.37	−0.27	0.02

Bold and italic fonts indicate the significance level at 0.05 and 0.01 level, respectively

Table 4 Number of stations showing positive and negative trends of temperature indices based on normalized test statistic *Z*

Index	Number of stations		Regional mean	
	Positive *Z*	Negative *Z*	*Z*	Decadal change
Extreme value indices				
TNn	26 (21)	–	**2.93**	1.35
TXx	21 (7)	5 (0)	0.92	0.13
Relative indices				
TN90p	26 (26)	–	**4.13**	6.80
TX90p	26 (25)	–	**2.57**	3.26
Absolute indices				
GSL	24 (19)	2 (0)	**2.93**	1.35
GDD	25 (25)	–	**2.42**	53.0

Numbers in parentheses indicate the number of stations with significant ($\alpha = 0.05$) trends. For the regional mean, normalized test statistic *Z* and decadal changes are shown with significant ($\alpha = 0.05$) trends indicated by bold face

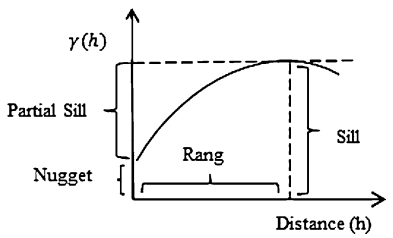

Fig. 2 Experimental semivariogram model

trend of local based spatial variability of the climate extreme indices.

2.2.3.3 Mapping The sequential regression kriging approach was employed to prepare maps by summing the maps produced by the multiple linear regression equation and kriging of the residuals, which were analyzed through

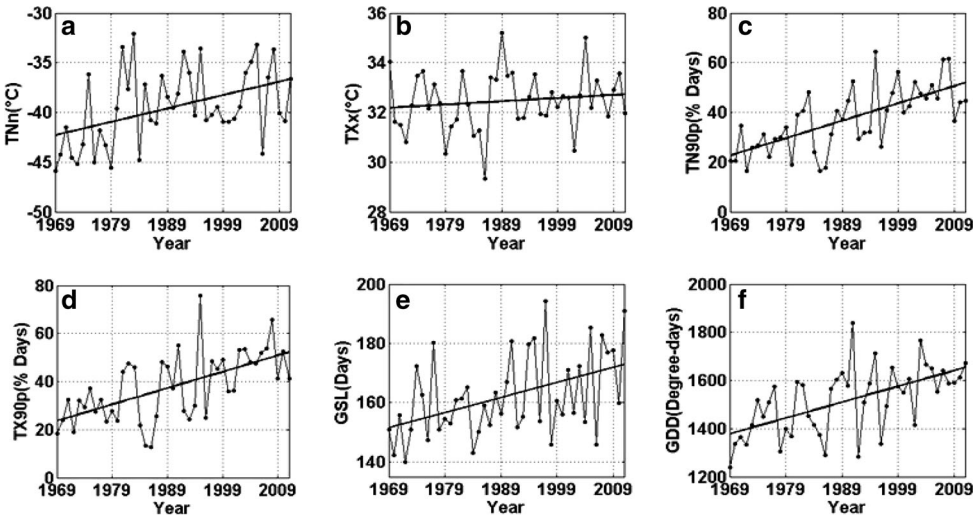

Fig. 3 Time series of the region level-averaged annual (**a**) *TNn*, (**b**) *TXx*, (**c**) *TN90p*, (**d**) *TX90p*, (**e**) GSL and (**f**) GDD, in the study area, 1969–2011

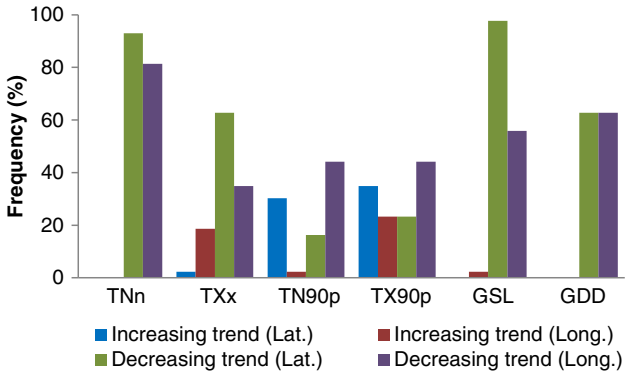

Fig. 4 Percentage of statistically significant ($\alpha = 0.05$) regional spatial trends for *TNn*, *TXx*, *TN90p*, *TX90p*, GSL and GDD from the computed spatial trend for the whole period (1969–2011)

the semivariogram function. The regression kriging equation can be written as:

$$z(s_o) = m(s_o) + e(s_o),$$

where $z(s_o)$ is the final predicted surface, $m(s_o)$ is the smoothed surface based on the multiple linear regression model, and $e(s_o)$ is the residuals surface interpolated through simple kriging.

Accordingly, maps of climate extreme indices were prepared for the period (1971–2000) as the reference period, and for the period (2031–2050) as the future scenario. Furthermore, the change of the spatial trend of the climate extremes between the two periods was computed in order to identify areas which will be affected more by climate extremes.

3 Results

The analysis of the temperature- and precipitation-based climate extreme indices reveal a variety of changes during the observed (1969–2011) and the projected (2021–2050) periods.

3.1 Temporal and spatial trends of temperature-based climate extremes

3.1.1 Extreme value indices

The analysis of the two extreme-value indices, *TNn* and *TXx*, based on the observed data (1969–2011) as shown in Table 3, exhibits an upward linear trend of 26 stations for *TNn* and of 21 stations for *TXx*. However, only 21 stations for *TNn* and 7 stations for *TXx* are significance at the $\alpha = 0.05$ level. Downward trends were observed for *TXx* for five stations, however, none of them is significant. The linear trend of *TNn* ranges from 0.07 to 0.18 °C year^{-1}. For *TXx*, the maximum increase reaches 0.06 °C year^{-1}, which is quite small as compared to the *TNn* values.

Regionally computed trends for *TNn* and *TXx* show increases, however, only *TNn* is significant at the 0.05 level (Table 4). The regional decadal trend for *TNn* is 1.35 °C and for *TXx*, it is 0.13 °C for the last 40 years. The time series graphs for the two indices depict that *TNn* increases sharply while *TXx* increase slightly during the study period (Fig. 3a, b). Additionally, the temporal variability decreases with time for *TXx*, especially during the recent decade.A semivariogram can be depicted as:

The spatial regional trend of the indices is presented in Fig. 4. *TNn* shows a decreasing trend along latitude and longitude in 90 and 80 % of the study period, respectively. *TXx* shows both increasing and decreasing trends along both latitude and longitude, however, most significant trends are decreasing along latitude (60 % of the study period) and along longitude (35 %). This analysis shows

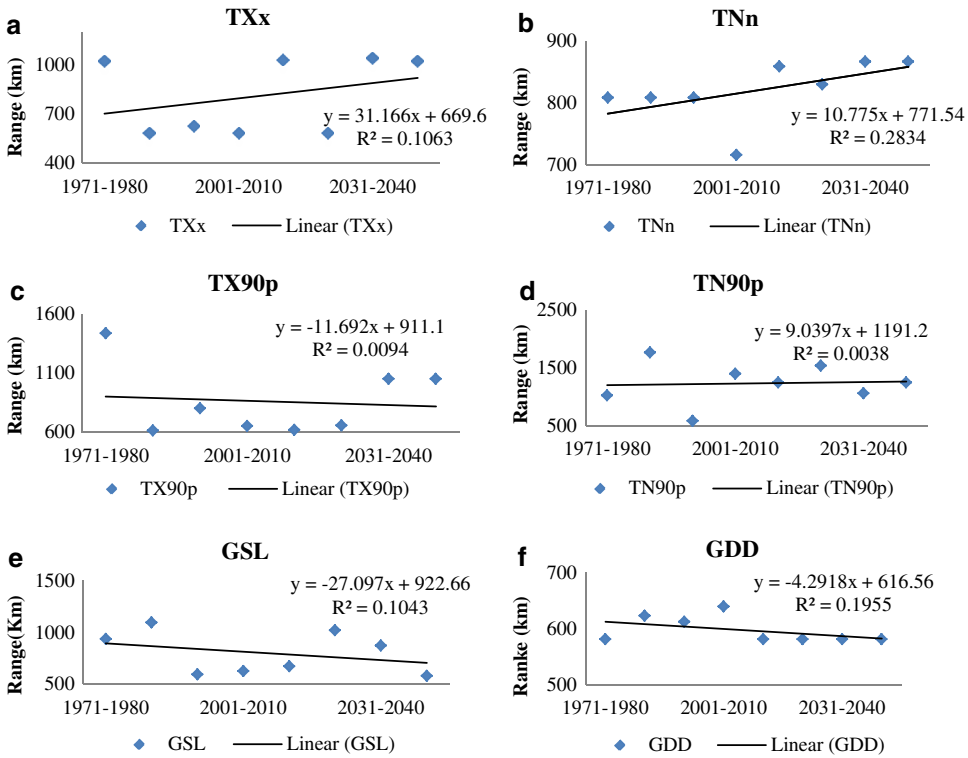

Fig. 5 Linear trend of range value of a semivariogram for (**a**) *TXx*, (**b**) *TNn*, (**c**) *TX90p*, (**d**) *TN90p*, (**e**) GSL and (**f**) GDD

that the southern part of the study region is experiencing a higher increasing rate of these indices than the northern part.

The local spatial trend of these indices, which is computed based on the range parameter of a semivariogram (covariance) function, shows an increasing trend during the whole study periods (Fig. 5a, b). On average, the range value of *TNn* increases by 10.7 km per decade and the range value of *TXx* increases by 31.1 km per decade. This implies that the spatial variability of these climate extreme indices is decreasing with time.

The relative change of these climate extreme indices in the future (2021–2050) with respect to the reference period (1971–2000) is mapped in Fig. 6. TN_n is projected to change from 6 to 19 %. The highest change is observed in the North-Western section of the region and the lowest in the SW section. In contrary, *TXx* is projected to change up to 12 % in the south-east and by 7.8 % in the north of the region. This rather complex spatial pattern implies that the intensity of warming varies strongly from place to place.

3.1.2 Relative indices

For *TN90p* and *TX90p*, an upward trend is observed for all stations in the study area (Table 3). Twenty six stations for *TN90p* and 25 stations for *TX90p* show significant increases at the $\alpha = 0.05$ level. The trend of *TN90p* ranges from 0.6 to 0.94 % days per year and the trend of *TX90p* ranges from 0.35 to 0.93 % days per year.

Regionally, both indices show a significant upward trend at the $\alpha = 0.05$ level (Table 4). *TN90p* increases at a decadal rate of 6.80 % days per decade while *TX90p* increases by 3.26 % days per decade, which is half of the *TN90p* rate. The time series graph of both indices (Fig. 3) show a sharp upward trend and the variability decreases for the last decade of the analysis period.

The spatial regional trend of these two indices (Fig. 4) exhibit both increasing and decreasing trends both along latitude and longitude, respectively. However, the combined frequency of significant trends along either axis is less than 50 % of the study period. This implies that there is no dominant directional trend for both indices.

Locally, the spatial variability of *TX90p* increases while the spatial variability of *TN90p* decreases. These trends are interpreted from the downward trend of the range value of *TX90p* and the upward trend of the range value *TN90p* as depicted by Fig. 5c, d, respectively. The range value for *TN90p* increases by 9 km per decade so that more area correlated with each other from time to time. In contrary, the range decreases for *TX90p* by −11.7 km per decade, implying that more area falls out from the correlation range so that variability increases.

3.1.3 Absolute indices

The GSL shows an upward trend for 24 stations (Table 3). For 19 stations, this trend is significant at the $\alpha = 0.05$ level. All stations show an upward trend for GDDs at the

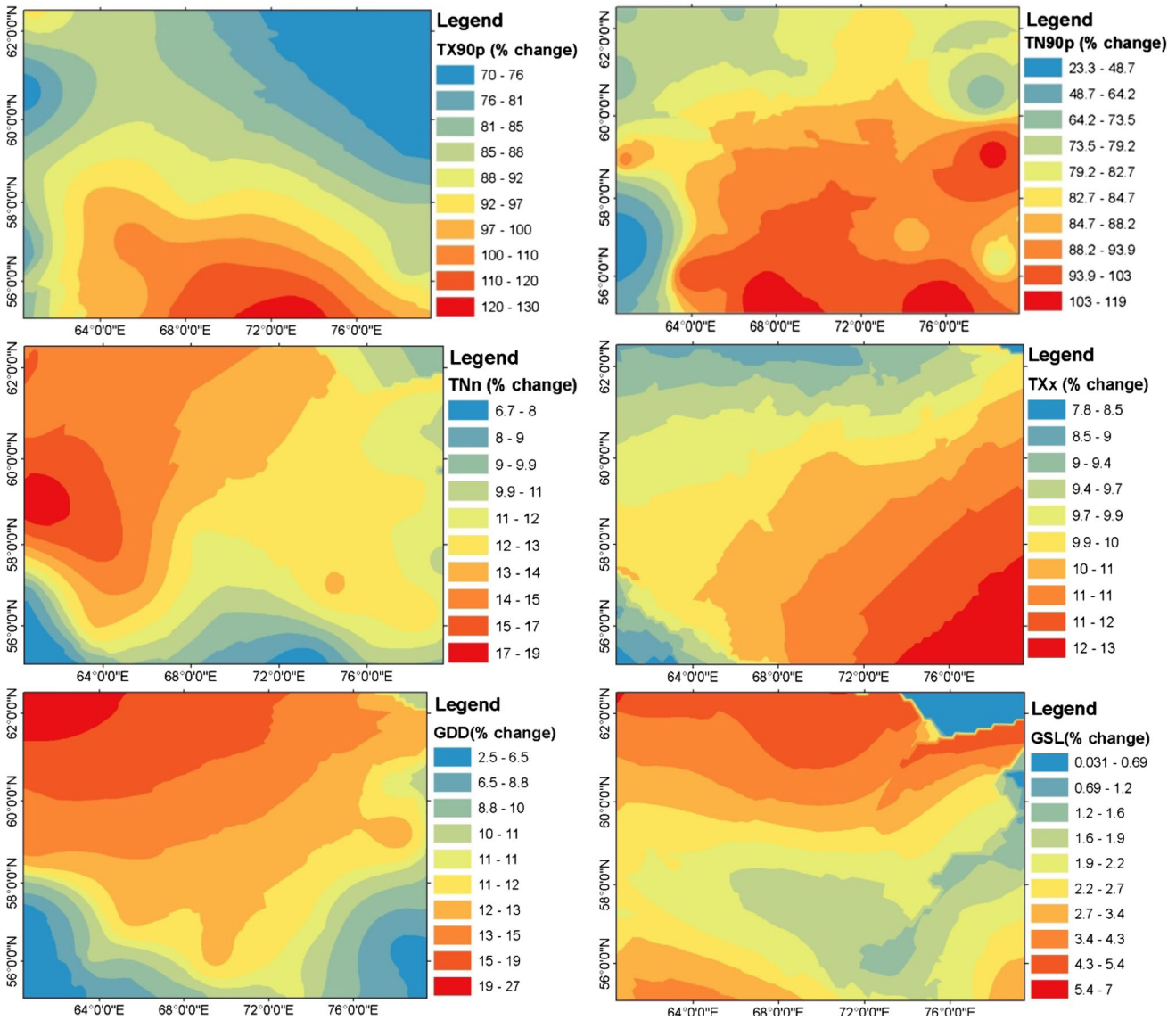

Fig. 6 Maps for percent change for *TX90p*, *TN90p*, *TNn*, *TXx*, GDD and GSL in the future (2021–2050) with respect to reference period (1971–2000)

Table 5 Number of stations showing positive and negative trends of precipitation indices based on normalized test statistic *Z*

Index	Number of stations		Regional mean	
	Positive *Z*	Negative *Z*	*Z*	Decadal change
Relative indices				
R95p	14 (0)	12 (0)	−0.78	−0.17
Absolute indices				
R10	17 (1)	9 (1)	−1.04	−0.01
R×5day	9 (1)	17 (1)	−1.64	−0.9
CDD	11 (0)	15 (0)	−0.13	−2.19

Number in parentheses indicates number of stations with significant trend at 0.05 levels. For the regional mean, normalized test statistic *Z* and the decadal changes are shown

$\alpha = 0.05$ significance level (Table 3). The highest value of GSL and GDD are 0.88 days year^{-1} and 8.14 degree-days year^{-1}, respectively.

In the regional analysis, the GSL and GDD increase upward at decadal rate of 1.35 days per decade and 53 degree-days per decade, respectively. The time series graph of GSL and GDD also illustrate the increase of both indices (Fig. 3e, f). Moreover, the decrease of the temporal variability of GDD is also depicted especially in the recent decade.

Both indices show a decreasing trend along latitude and longitude in more than 50 % of the study period (Fig. 4). This implies that the southern part of the study area is undergoing a higher increase of these indices than the

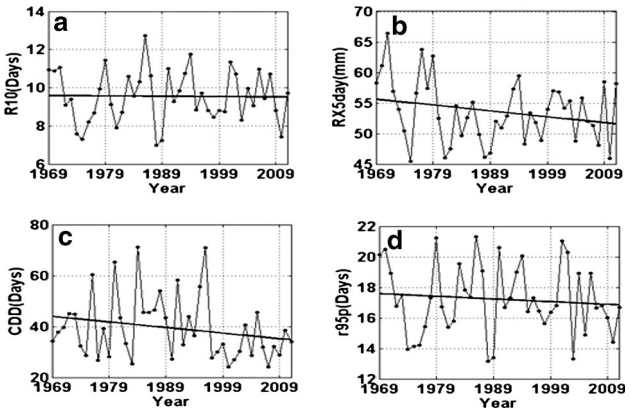

Fig. 7 Time series of the region level-averaged annual (**a**) *R10*, (**b**) *RX5day*, (**c**) CDD and (**d**) *R95p*, in the study area, 1969–2011

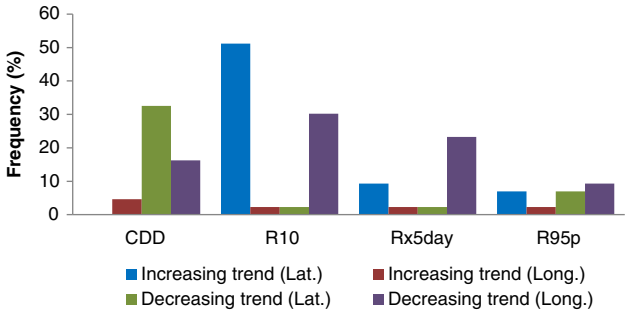

Fig. 8 Percentage of statistically significant ($\alpha = 0.05$) regional spatial trend for CDD, *R10*, *R×5day* and *R95p* from the computed spatial trend for the whole period (1969–2011)

northern region. Furthermore, the local spatial variability of these indices increases with time as it is depicted in Fig. 5e, f by the downward trend of the respective range values.

Up to 7 % change for GSL and 27 % change for GDD are expected in the future period (2021–2050) with respect to the reference period (1971–2000) in the most northern part of the region.

3.2 Temporal and spatial trend of precipitation based climate extremes

Table 5 shows the precipitation indices that are categorized into a relative precipitation index (*R95p*) and absolute precipitation indices (*R10*, *R×5day*, CDD, SDII). No significant trend is observed in any of these indices at the regional level. However, very few stations show significant trends for various indices.

3.2.1 Relative indices

Nearly equal numbers of stations show an upward and downward trend for the *R95p* index, respectively (Table 3). Fourteen stations show upward trends and 12 stations show downward trends. However, none of them are significant at the $\alpha = 0.05$ level. The linear trend value ranges from -0.08 to 0.1 days year^{-1}.

The regional trend of *R95p* is downward at -0.17 days year^{-1}. However, the trend is not significant as well (Table 5).

The time series graph of this index exhibits a slight downward trend. The very large variability of values, which is apparent for the time period before the 1990s, is reduced afterwards (Fig. 7d).

Spatially, there is no dominant direction for the regional trend of *R95p* along longitude and latitude. The increasing and/or decreasing trends of this index in both dimensions occur during less than 10 % of the study period (Fig. 8). However, the local variability is reduced as shown by the increasing trend of the range value of the index (Fig. 9). This increase amounts to 310 km per decade. In other words, the numbers of stations that are spatially correlated are increasing with time.

The 40 years mean spatial pattern of R_{95p} shows that the highest *R95p* occurs in a small pocket of land in the south-eastern part of the study area, and the lowest value occurs in SW part of the study area (Fig. 10).The middle and northern part of the region are experiencing moderate values of the *R95p* index.

3.2.2 Absolute indices

R10, *R×5day* and CDD are the indices which are categorized as absolute indices. Station-based analysis of these indices shows that there are upward and downward trends with only a very few stations showing trends significant at the $\alpha = 0.05$ level (Table 3). For the *R10* index, 17 stations show an upward trend and 9 stations show a downward trend. Only two trends, one of either direction, are significant at the $\alpha = 0.05$ level. The highest value reaches to 0.09 days year^{-1}. The regional trend for *R10* is downward but not significant as well. It amounts -0.01 days per decade. For *R×5day*, the same numbers of stations as in the case of *R10* show trends. However, the trend direction is opposite. Again, only two stations show significant trends, one of either direction. The *R×5day* linear trend value ranges from -0.58 to 0.3 mm year^{-1} and the regional trend is -0.9 mm per decade.

Regarding CDD, 11 stations show upward trend and 15 stations show downward trend. None of the trends are significant for CDD. Its linear trend value ranges from -0.37 to 0.2 days year^{-1}. No significant trend also observed for CDD at the regional level (Table 5). Its trend value amounts -2.19 days per decade. The variability of *R10*, *R×5day*, and CDD apparently decrease after the year 2000 (Fig. 7a–c). The regional spatial trend for *R10*

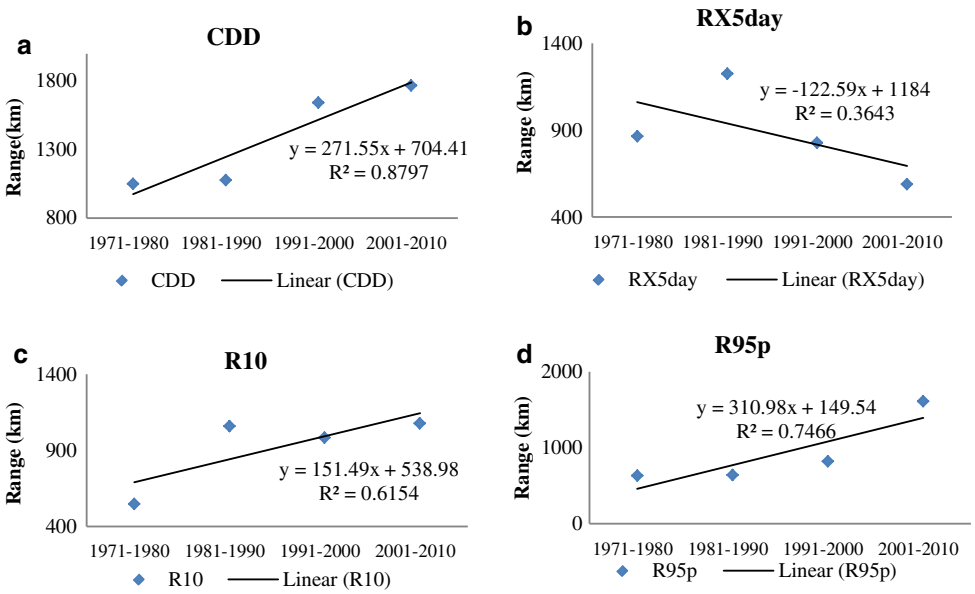

Fig. 9 Linear trend of range value of a semivariogram for (**a**) CDD, (**b**) *R×5day*, (**c**) *R10* and (**d**) *R95p*

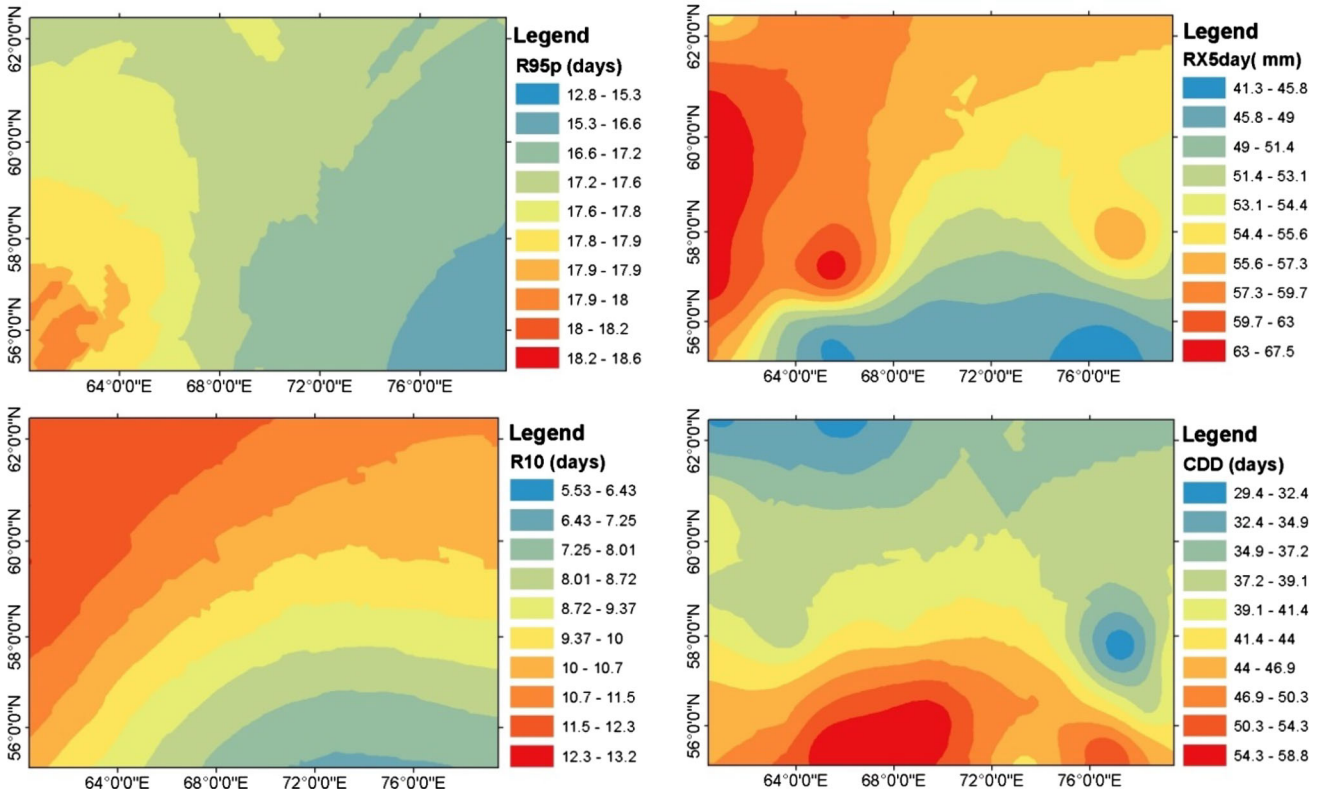

Fig. 10 Mean spatial pattern of *R95p*, *R×5day*, R_{10} and CDD in the past (1969–2011)

exhibits an increasing trend along latitude in nearly 50 % of the analysis period, and a decreasing trend along longitude during 30 % of the analysis period (Fig. 8). For CDD, the decreasing trend along latitude is relatively dominant and amounts nearly 30 % of the study period.

The *R10* and CDD indices exhibit an increase of range value with a linear trend of 251 and 271 km per decade, respectively (Fig. 9a, b).This implies that more stations are becoming correlated to each other over time. For *R×5day*, the range value rather decreases at a linear rate of

−122 km per decade. In other words, local variability increases with time for this index.

For the mean spatial pattern for *R10*, the highest value 13.2 days year^{-1} occurs in the North-Western part and it decreases to the south-east to the value of 5.5 days year^{-1} (Fig. 10). The *R×5day* follow a similar pattern except very few pocket areas experiencing higher values. The highest value in the east part of the study area reaches to 67.5 mm year^{-1}. In contrary, the highest CDD values are found in the southern part of the study area. However, small pockets of land in the south also experience a lower CDD value. The Highest CDD value reaches to 58.8 days year^{-1} and the lowest reaches to 29.4 days year^{-1}.

4 Discussion and conclusion

The analysis of various climate extreme indices based on the observed and projected climate data have evidenced significant upward trends for most of temperature-based indices while the precipitation-based climate extremes indices showed no significant trend at all. This mirrors studies at the global level that also found that precipitation-based extremes are less significant than those based on temperatures (Alexander et al. 2006).

The regional time series graphs of the climate extreme indices reveal that the variability is decreasing through time for most indices, especially during the last decades or after 2000. This decrease in temporal variability of the climate indices is also reflected by the decrease of the spatial variability through time for most indices, as indicated by the increasing trend of the range value of the semivariogram function computed for individual climate extreme indices. This decrease of variability implies that a larger area is becoming similar, meaning that the study area becoming more homogenous. This tendency may indicate that the large-scale atmospheric patterns are becoming more dominant as compared to the local factors which are responsible for variations of the climate extremes at local level. An earlier study for the area showed that the large scale atmospheric pattern, Arctic Oscillation, explains 53 % of temperature variation in Western Siberia (Frey and Smith 2003).

The regional spatial pattern of the climate extreme analysis shows that the temperature-based climate extremes, *TNn*, *TXx*, GSL and GDD, decrease while the precipitation-based climate extremes, *R10* and *R×5day*, increase along latitude and longitude for more than half of the analysis period. Relatively, the southern part of the region becomes drier and warmer and the northern part becomes wetter and less warmer compared to the south. The higher value and frequency of the CDD index confirms that the southern region experiences more drought events as well. Hence, it is apparent that the southern part of the study area, which is classified as forest steppe, is influenced more by environmental stress than areas in the north, the pre-Taiga and south Taiga. This tendency indicates the potential effect of climate change to foster a northward shift of the West-Siberian grain belt into the forest steppe and pre-Taiga zone in addition to the landuse/cover change that is the main driver in the area. This reasoning is further confirmed by the larger change of the projected bio-climate indicators, length of the growing season (GSL) and GDDs, in the north.

In relation to the climate extremes, some finger prints of extreme events have been observed in the region during recent decades. For instance, the fire risk intensity increased in the study region during the last decade (Balzter et al. 2010; Stocks et al. 1998). Forest fires lead to the release of enormous amounts of stored carbon into the atmosphere. Besides the forests, peatlands are also affected by fire causing significant losses of carbon (Houghton 2003; Wirth et al. 2002; Schulze and Freibauer 2005). Moreover, indications of agricultural drought in the southern steppe part of the study region were reported by researchers working in the area. In response, field experimentation of drought-resistant varieties (e.g., wheat) has been initiated during the last few years.

All in all, this study presents the temporal and spatial pattern of climate extremes. The changes in intensity and frequency of climate extremes are becoming the main threat for the region. Various ecosystems in the area are negatively affected.

The statistical approach which is used in this study opens the possibility to analyze the spatio-temporal dynamics of climate extremes at local and regional scales and in long-term data sets combining past and projected future time periods. As a result, specific and rather precise recommendations can be developed for agriculture, forest management, and protection of nature and biodiversity, which can be used to develop climate change adaptation strategies.

Acknowledgments This work was conducted as part of Project SASCHA ('Sustainable land management and adaptation strategies to climate change for the Western Siberian corn-belt'). We are grateful for funding by the German Government, Federal Ministry of Education and Research within their Sustainable Land Management funding framework (funding reference 01LL0906D). Degefie T. Degefie received additional funding by the German Academic Exchange Service (DAAD). We thank the two anonymous reviewers for very helpful comments on an earlier version of the manuscript.

References

Alexander LV, Zhang X, Peterson TC, Caesar J, Gleason B, Tank MGK, Haylock M, Collins D, Trewin B, Rahimzadeh F, Tagipour A, Rupa Kumar K, Revadekar J, Griffiths G, Vincent

L, Stephenson DB, Burn J, Aguilar E, Brunet M, Taylor M, New M, Zhai P, Rusticucci M, Vazquez-Aguirre JL (2006) Global observed changes in daily climate extremes of temperature and precipitation. J Geophys Res 111:D05109. doi:10.1029/2005JD006290

Arnone JA, Verburg PSJ, Johnson DW, Larsen JD, Jasoni RL, Lucchesi AJ, Batts CM, von Nagy C, Coulombe WG, Schorran DE, Buck PE, Braswell BH, Coleman JS, Sherry RA, Wallace LL, Luo Y, Schimel DS (2008) Prolonged suppression of ecosystem carbon dioxide uptake after an anomalously warm year. Nature 455(7211):383–386

Balzter H et al (2010) Environmental change in Siberia: earth observation, field studies and modeling. In: Balzter H (ed) Advances in global change research, vol 40. Springer, Dordrecht. doi:10.1007/978-90-481-8641-9_2

Frey KE, Smith LC (2003) Recent temperature and precipitation increases in West Siberia and their association with the Arctic Oscillation. Polar Res 22:287–300

Gemmer M, Fischer T, Jiang T (2011) Trends in precipitation extremes in the Zhujiang River Basin, South China. J Clim 24:750–761

Houghton RA (2003) Revised estimates of the annual net flux of carbon to the atmosphere from changes in land use and land management 1850–2000. Tellus B 55:378–390

IPCC (2007a) In: Parry ML, Canziani OF, Palutikof JP, van der Linden PJ, Hanson CE (eds) Climate change 2007: impacts, adaptation and vulnerability. Contribution of Working Group II to the Fourth Assessment Report of the Intergovernmental Panel on Climate Change. Cambridge University Press, Cambridge

IPCC (2007b) Summary for policymakers. In: Solomon S, Qin D, Manning M, Chen Z, Marquis M, Averyt KB, Tignor M, Miller HL (eds) Climate change 2007: the physical science basis. Contribution of Working Group I to the Fourth Assessment Report of the Intergovernmental Panel on Climate Change. Cambridge University Press, Cambridge

IPCC (2012) In: Field CB, Barros V, Stocker TF, Qin D, Dokken DJ, Ebi KL, Mastrandrea MD, Mach KJ, Plattner G-K, Allen SK, Tignor M, Midgley PM (eds) Managing the risks of extreme events and disasters to advance climate change adaptation. A Special Report of Working Groups I and II of the Intergovernmental Panel on Climate Change. Cambridge University Press, Cambridge

Kendall MG (1975) Rank correlation methods. Griffin, London

Kharin V, Zwiers FW, Zhang X, Hegerl GC (2007) Changes in temperature and precipitation extremes in the IPCC ensemble of global coupled model simulations. J Clim 20(8):1419–1444

Mann HB (1945) Nonparametric tests against trend. Econometrica 13:245–259

Pilifosova O, Eserkepova I, Dolgih S (1997) Regional climate change scenarios under global warming in Kazakhstan. Clim Change 36:23–40

Schulze ED, Freibauer A (2005) Environmental science—carbon unlocked from soils. Nature 437:205–206

Shulgina TM, Genina EYu, Gordov EP (2011) Dynamics of climatic characteristics influencing vegetation in Siberia. Environ Res Lett 6:045210

Stocks BJ, Fosberg MA, Lynham TJ, Mearns L, Wotton BM, Yang Q, J-Z Jin, Lawrence K, Hartlet GR, Mason JA, McKenney DW (1998) Climate change and forest fire potential in Russian and Canadian boreal rorests. Climatic Change 38:1-1

Vincent LA et al (2011) Observed trends in indices of daily and extreme temperature and precipitation for the countries of the western Indian Ocean, 1961–2008. J Geophys Res 116:D10108. doi:10.1029/2010JD015303

Wang W, Shao Q, Yang T, Peng S, Yu Z, Taylor J, Xing W, Zhao C, Sun F (2012) Changes in daily temperature and precipitation extremes in the Yellow River Basin, China. Stoch Environ Res Risk Assess Springer. doi:10.1007/s00477-012-0615-8

Wirth C, Czimczik CI, Schulze ED (2002) Beyond annual budgets: carbon flux at different temporal scales in fire-prone Siberian Scots pine forests. Tellus B 54:611–630

WMO (2009) In: Klein Tank AMG, Zwiers FW, Zhang X, Royal Netherlands Meteorological Institute (eds) Guidelines on Analysis of extremes in a changing climate in support of informed decisions for adaptation. Environment Canada

Yang T, Wang X, Zhao C, Chen X, Yu Z, Shao Q, Xu C-Y, Xia J, Wang W (2011) Changes of climate extremes in a typical arid zone: observations and multimodel ensemble projections. J Geophys Res 116:D19106. doi:10.1029/2010JD015192